

Synthesis of 3,4-dimethoxythiophene spacer-based non-fullerene acceptors for efficient organic solar cells

Ie Na Kim, Sung Jae Jeon, Young Hoon Kim, Hyoung Seok Lee, Yong Woon Han, Nam Gyu Yang, Dong Hyeon Hong, Chang Ho Jung, Doo Kyung Moon*

Nano and Information Materials (NIMs) Laboratory, Department of Chemistry Engineering, Konkuk University, 120, Neungdong-ro, Gwangjin-gu, Seoul 05029, South Korea

ARTICLE INFO

Keywords:

Organic solar cells
Non-fullerene acceptors
3,4-Dimethoxythiophene
Up-shifted LUMO energy level

ABSTRACT

Three narrow bandgap non-fullerene acceptors (NFAs) named as IDTT2OT, IDTT2OT-2F, and IDTT2OT-4F were designed and synthesized using a 3,4-dimethoxythiophene as a π -spacer linking the indacenodithieno[3,2-*b*]thiophene (IDTT) core and 2-(3-oxo-2,2,3-dihydroinden-1-ylidene) (IC) end groups. The NFAs exhibited relatively narrow bandgaps (1.51, 1.45, and 1.42 eV) and up-shifted unoccupied molecular orbital (LUMO) energy levels (-3.69, -3.83, and -3.90 eV) owing to the 3,4-dimethoxythiophene effect compared with the similar structures. By finely tuning the energy levels modulation with a poly[2,6-4,8-bis(5-(2-ethylhexyl)thiophen-2-yl)-benzo-1,2-*b*:4,5-*b'*]dithiophene]-alt-(5,5-(1,3'-di-2-thienyl-5',7'-bis(2-ethylhexyl)benzo[1',2'-*c*:4',5'-*c'*]dithiophene-4,8-dione)) (PBDB-T) donor, all the NFA-based devices showed the broad photo-responses, at 300–900 nm, with small energy losses of 0.56–0.58 eV, and thus enhanced the light-harvesting ability of organic solar cells (OSCs). Among the NFA-based blends, the PBDB-T:IDTT2OT-4F device exhibited the best power conversion efficiency (PCE, 10.40%) with a high short-circuit current density (J_{SC}) of 19.3 mA cm⁻² and an open-circuit voltage (V_{OC}) of 0.86 V. Our results demonstrate that introducing 3,4-dimethoxythiophene is an efficient strategy for improving the electron accepting ability of NFAs by tuning frontier energy levels.

1. Introduction

With their capacity for conversion of solar light into electricity, organic solar cells (OSCs) have been studied extensively in recent decades owing to their advantages of low cost, light weight, and flexibility [1–7]. Previous studies have revealed that fullerene acceptors, although possessing strong electron mobilities and affinities, suffer from various drawbacks, including weak absorption in the visible and near-infrared (NIR) regions and a limited structural modification potential [7–11]. By contrast, non-fullerene acceptors (NFAs), containing electron withdrawing components such as benzothiadiazole, benzodithiophene, etc., allow simple energy level modulation and control of the absorption area through molecular design, hence NFAs development has accelerated rapidly [2,6–16]. In particular, the acceptor–donor–acceptor (A–D–A) NFAs, consisting of a fused electron-donating core and strong electron-withdrawing end groups, effectively transport charge carriers via the push-pull effect, and their energy levels can be easily modified by varying the moieties within their structures [7–12,17–19]. Thanks to

these merits, the efficiencies of OSCs have been increased by the incorporation of A–D–A NFAs, the energy levels of which can be adjusted to generate suitable offsets and enhance light-absorption matching with the donor [2,7,13,15,16].

The molecular designs of NFAs suggest various possibilities for further increases in the efficiency of NFA-based OSCs. Nowadays, narrow bandgap (< 1.5 eV) NFAs, which can absorb the in NIR region, are being actively investigated because of their strong light-harvesting abilities [11,12,17,18]. As NIR region accounts for 50% of the total solar radiation intensity [7], the development of narrow-bandgap NFAs is desirable for enhanced current generation and increased short-circuit current density (J_{SC}) [6,9,12,18].

For the design of A–D–A type NFAs, the introduction of π -spacer unit is a relatively straightforward method, when compared with the synthesis of fused-ring extensions to increase π -conjugation [20,21]. For examples, benzotriazole, quinoxaline and thieno[3,4-*C*]pyrrole-4,6-dione are widely used π -spacers for their weak electron accepting ability which can lower the lowest unoccupied molecular orbital

* Corresponding author.

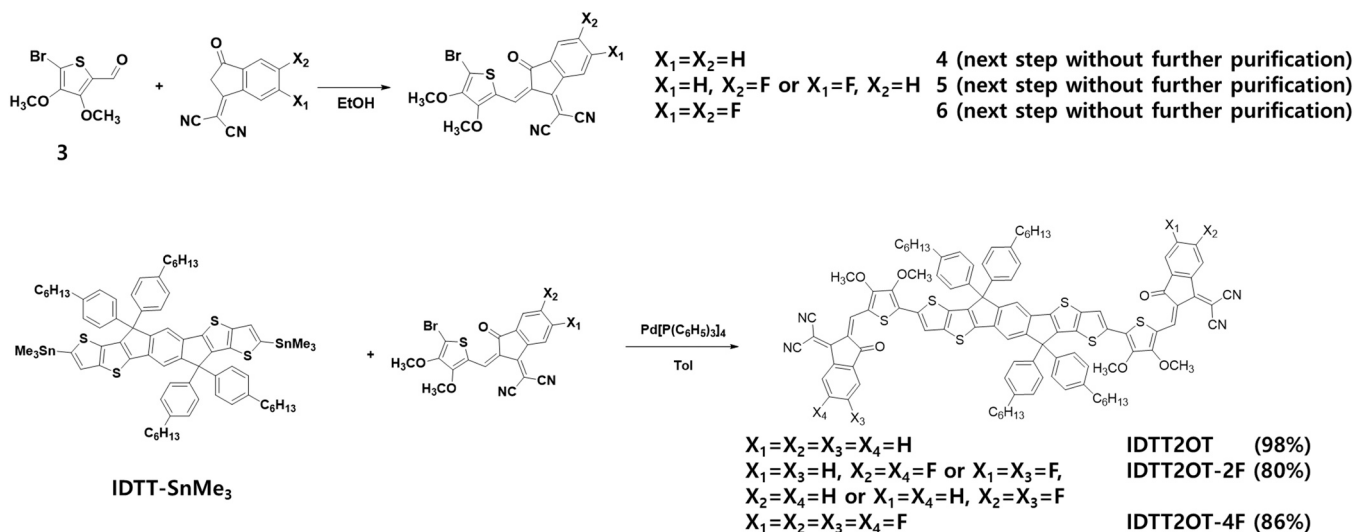
E-mail address: dkmoon@konkuk.ac.kr (D.K. Moon).

<https://doi.org/10.1016/j.synthmet.2021.116880>

Received 9 June 2021; Received in revised form 3 August 2021; Accepted 6 August 2021

Available online 26 August 2021

0379-6779/© 2021 Published by Elsevier B.V.



Scheme 1. Synthetic route for IDTT2OT, IDTT2OT-2F, and IDTT2OT-4F.

(LUMO) level, lowering the band gap energy of NFAs [22–26]. Through a couple of additional synthetic steps using various π -spacers, an A- π -D- π -A configuration can be created from A-D-A structure to modulate the energy levels of NFAs with well-characterized central donor units. In addition, an atom with strong electronegativity in the spacer such as oxygen can be connected to other units through non-covalent interactions, facilitating planarization and intramolecular charge transfer [17,27–29]. Thus, all the effects that stem from adopting the spacer unit efficiently reduce the energy bandgap and enhance the NIR photo-response, thereby achieving higher J_{SC} for the OSC device [6].

However, there is a trade-off between the effective charge separation, which aids photocurrent generation, and voltage loss by strong non-radiative recombination in the cell [17,30]. The open-circuit voltage (V_{OC}) in an OSC device is primarily determined by the adequacy of the charge-transfer state energy [31]. When an increased J_{SC} can be obtained, a smaller offset between the LUMO level of the acceptor and the highest occupied molecular orbital (HOMO) level of the donor molecule might induce a reduction in V_{OC} [32,33]. For instance, J_{SC} enhancement achieved via broadening the NIR absorption band by decreasing the LUMO level often reduces V_{OC} [18]. Therefore, precise engineering of the frontier energy levels of active materials is required to obtain devices with desirable J_{SC} and V_{OC} values, and consequently, remarkable PCEs. To this end, up-shifting LUMO level of NFAs is a good option for elevating J_{SC} without compromising on V_{OC} . In this strategy, decreased HOMO offset helps increase the gap between the acceptor LUMO and donor HOMO, thereby increasing V_{OC} and diminishing the energy loss, which is defined as the $E_{loss} = E_g^{opt} - eV_{OC}$, where E_g^{opt} is the optical bandgap [11,18,34–39].

For example, Zhan et al. proved that adopting a 3,4-dimethoxythiophene spacer on NFA (IEICF-DMOT) is an efficient strategy for lifting LUMO level up comparing with an IEICO-4F acceptor which possess long branched alkoxy chain on thiophene spacer at 3-position. Up-shifted LUMO level of IEICF-DMOT effectively closed the energy offset with PBDB-T donor and exhibited higher device performance (9.98–13.01%), increase of V_{OC} (0.74–0.87 V) with reasonable NIR absorption (23.10–22.14 mA cm⁻²) for its enlarged energy bandgap than IEICO-4F based device [28].

Moreover, Chen et al. strengthened the electron-donating ability of an acceptor by incorporating a thiophene spacer between indacenodithieno[3,2-b]thiophene (IDTT) core and 2-(3-oxo-2,2,3-dihydroinden-1-ylidene) (IC) end groups. ITTIC exhibited increased LUMO energy from -4.00 to -3.82 eV and the HOMO level from -5.55 to -5.28 eV, when compared with ITIC. The narrow bandgap (1.46 eV) achieved with the

elevated LUMO level for ITTIC corresponded to a larger V_{OC} of 0.92 V and a broader photo-response, with a J_{SC} of 15.93 mA cm⁻², reduced energy loss (0.54 eV), and PCE of 9.12%, which is higher than that of the ITIC-based device [12].

Taking advantage of those strategies, we aim to raise the LUMO level and narrow its energy bandgap under 1.5 eV simultaneously through introducing a spacer, which is a suitable strategy for effective NIR absorption with minimizing voltage loss of the device. A shortest dialkoxy-functionalized thiophene spacer with planar IDTT core and IC end groups could be an effective approach to lift the LUMO energy level up and smaller the bandgap of NFAs without causing unexpected steric hindrance and altered intermolecular packing.

Herein, by introducing 3,4-dimethoxythiophene as spacer, new NFAs—IDTT2OT, IDTT2OT-2F, and IDTT2OT-4F—were designed and synthesized with the aim of precisely tuning the frontier energy level by differentially fluorine-substituted end groups. For these three acceptors, low E_g^{opt} values of 1.51, 1.45, and 1.42 eV are obtained with increased LUMO energy levels of -3.69, -3.83, and -3.90 eV, respectively, which are relatively high-lying LUMO levels than those of other NIR bandgap acceptors [17,28,40,41]. Further photovoltaic optimization revealed that IDTT2OT-4F based OSCs exhibited the best PCE of 10.40%, a reasonably high J_{SC} of 19.3 mA cm⁻², V_{OC} of 0.86 V, and a fill factor (FF) of 62.4% owing to the strong photo-response at 300–900 nm, with small E_{loss} of 0.56 eV.

2. Experimental section

2.1. Materials synthesis

Unless otherwise noted, all chemicals used in the syntheses were purchased from Aldrich, Alfa Aesar, Acros, or TCI, and used without further purification; (4,4,9,9-tetrakis(*p*-hexylphenyl)-4,9-dihydro-s-indaceno[1,2-*b*:5,6-*b'*]dithiophene-2,8-diyl)bis(trimethylstannane) (IDTT-SnMe₃) was purchased from Sunatech Inc. All reactions were performed under nitrogen atmosphere and checked by thin layer chromatography (TLC) on silica gel. Column chromatography was conducted using silica gel 60 (230–400 mesh ASTM, Merck).

IDTT2OT, IDTT2OT-2F, and IDTT2OT-4F were synthesized through Scheme 1; the synthetic details are given in the Supplementary material. With nucleophilic substitution of 3,4-dibromothiophene, 3,4-dimethoxythiophene (1) was synthesized with a yield of 61% (Notice: This liquid monomer is unstable due to the strong electron-donating character of alkoxy chain on thiophene, keep and handle carefully it on the refrigerator); 3,4-dimethoxythiophene-2-carbaldehyde (2) was

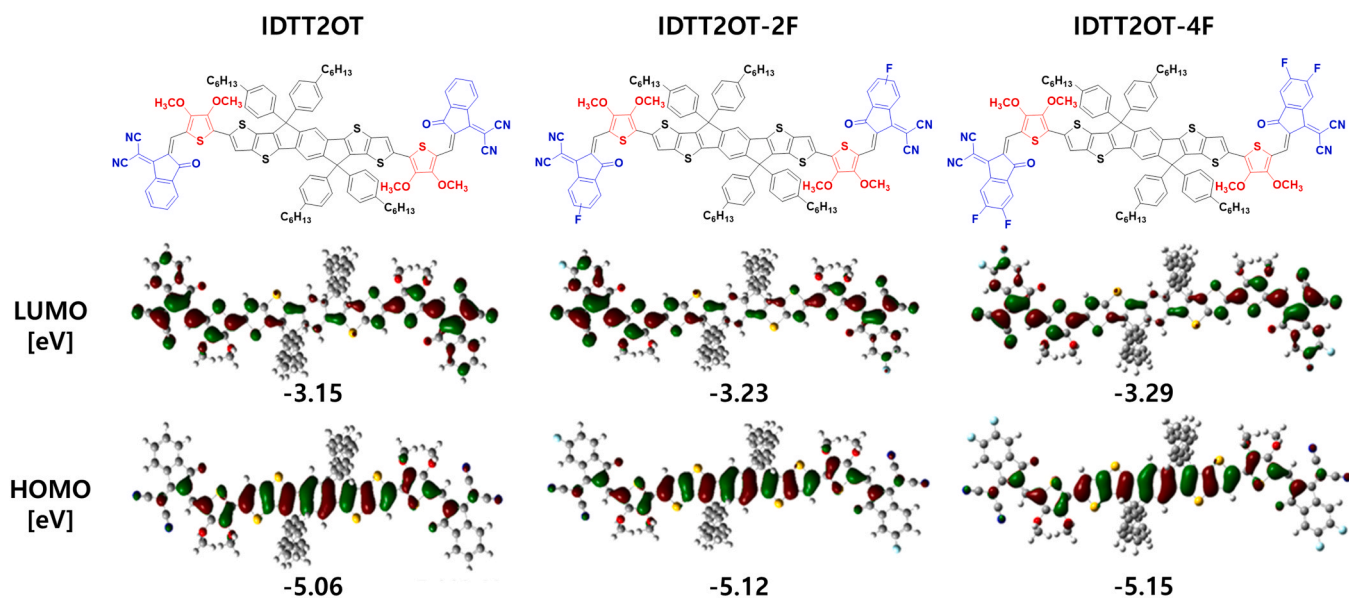


Fig. 1. Chemical structure and theoretical calculation of IDTT2OT, IDTT2OT-2F, and IDTT2OT-4F.

synthesized through the Vilsmeier–Haack reaction with a yield of 67% and 5-bromo-3,4-dimethoxythiophene-2-carbaldehyde (**3**) brominated with a yield of 75%. The OT-IC (**4**), OT-IC-F (**5**), and OT-IC-2F (**6**), were synthesized via Knoevenagel condensation by using (**3**), IC, IC-F, and IC-2F, respectively, and used without purification. Finally, IDTT2OT (**7**), IDTT2OT-2F (**8**), and IDTT2OT-4F (**9**) were synthesized through Stille coupling reaction between IDTT-SnMe₃ and (**4**), (**5**), and (**6**), with the palladium catalyst under toluene, with a yield of 98%, 80%, and 86%, respectively. The final products have more stable in chemical, owing to the structural stabilization would be formed compared to the 3,4-

dimethoxythiophene-based monomers [42,43]. The structure of the intermediate materials was characterized using ¹H NMR, and IDTT2OT, IDTT2OT-2F, and IDTT2OT-4F were fully characterized through ¹H NMR, ¹³C NMR (Figs. S1–S9), and MALDI-TOF. All NFAs are finely soluble in common solvents such as chloroform (CHCl₃), tetrahydrofuran (THF), chlorobenzene (CB) at room temperature.

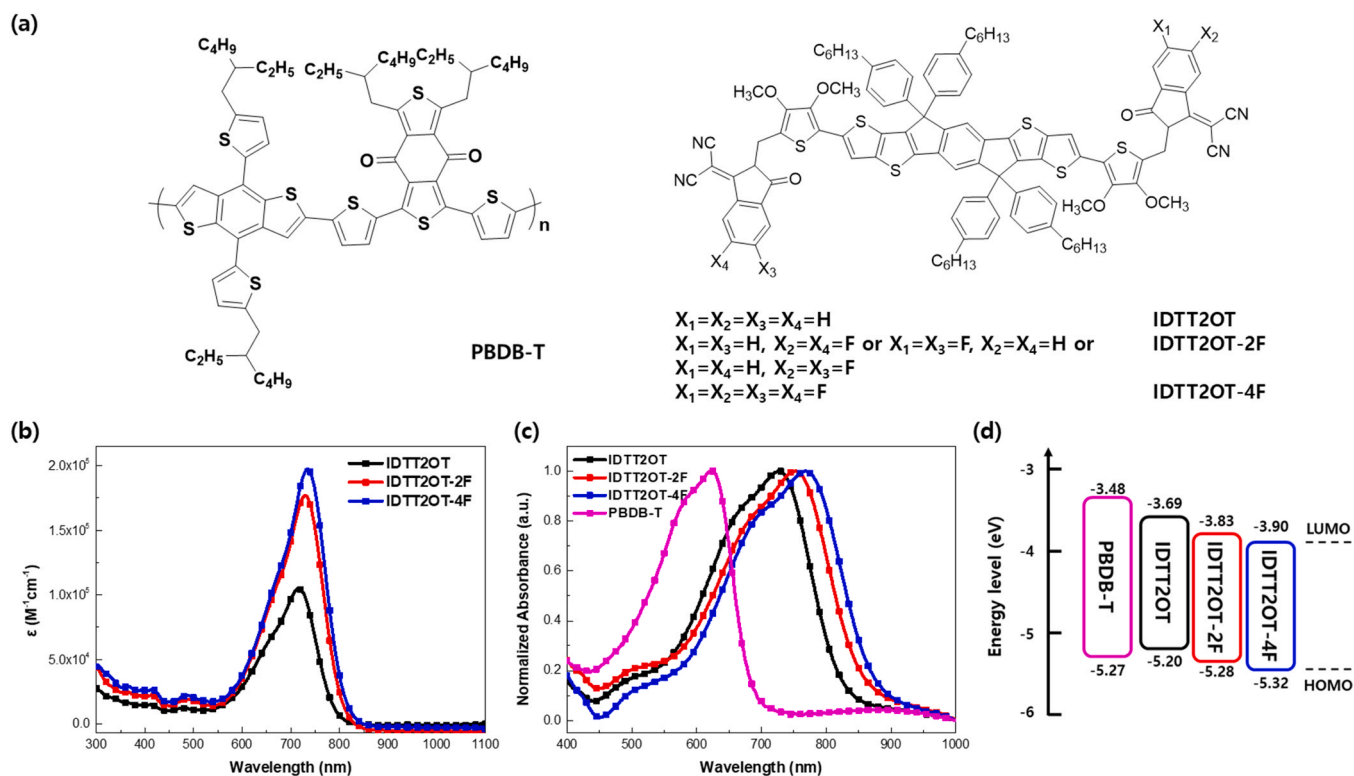


Fig. 2. (a) Molecular structures, (b) molar absorption coefficients in dilute chloroform solution, (c) UV-vis absorption spectra on thin films, and (d) energy level diagrams of PBDB-T, IDTT2OT, IDTT2OT-2F, and IDTT2OT-4F.

Table 1
Optical and electrochemical properties of IDTT2OT, IDTT2OT-2F, and IDTT2OT-4F.

NFAs	UV-vis absorption					CV	
	$\lambda_{\max, \text{sol}}$ [nm]	$\lambda_{\max, \text{film}}$ [nm]	λ_{onset} [nm]	$E_{\text{g}}^{\text{opt(a)}}$ [eV]	ϵ [$\text{M}^{-1} \text{cm}^{-1}$]	$E_{\text{HOMO}}^{\text{b)}$ [eV]	$E_{\text{LUMO}}^{\text{c)}$ [eV]
IDTT2OT	717	725	820	1.51	1.09×10^5	-5.20	-3.69
IDTT2OT-2F	731	754	856	1.45	1.77×10^5	-5.28	-3.83
IDTT2OT-4F	734	768	873	1.42	2.03×10^5	-5.32	-3.90

$$\text{a) } E_{\text{g}}^{\text{opt}} = 1240/\lambda_{\text{onset}}, \text{ b) } E_{\text{HOMO}} = - \left(\frac{E_{\text{onset}}^{\text{ox}} - E_1}{2}, \text{ferrocene} \right) - 4.8 \text{ eV}, \text{ c) } E_{\text{LUMO}} = E_{\text{HOMO}} - E_{\text{g}}^{\text{opt}}$$

3. Results and discussion

3.1. Theoretical simulation

Initially, density functional theory (DFT) calculations were carried out to evaluate the optimized energy levels and geometries of IDTT2OT, IDTT2OT-2F, and IDTT2OT-4F. ITTIC, which has no methoxy chains on the thiophene spacer, as reported by Chen et al., was also examined to better understand the electronic system (Fig. S10). For all NFAs, the HOMO energy mainly spread along the conjugated core, and the LUMO energy delocalized over the entire molecules, especially on the end groups (Fig. 1). Compared with ITTIC, IDTT2OT shows higher LUMO and HOMO by 0.12 and 0.14 eV, respectively, meaning the introduction of a dimethoxy chain is an effective strategy for narrowing the energy bandgap by raising the LUMO level of NFAs, which would result in enhanced V_{OC} in devices. As fluorination can occur at the two edges of an IC unit, the energy levels of the three isomers of IDTT2OT-2F, shown in Fig. S11, have the same HOMO but slightly different LUMO levels. IDTT2OT-4F exhibits the lowest frontier energy levels among the NFAs (Fig. 1), coincident with the effect of fluorination on the NFAs, which is

expected to lower the frontier energy levels and increase photon absorption in the longer wavelength region by narrowing the bandgap [44]. Furthermore, all three NFAs exhibit a small dihedral angle of $\sim 0.38^\circ$ between the flat IDTT core and spacer and $\sim 3.28^\circ$ between the end group and spacer (Fig. S12). With non-covalent interactions among the units as well as small dihedral angles and planar backbone, the strong intramolecular interactions and planar conformation of could be ascribed to an effective charge separation [14,45,46]. Due to its asymmetrical position of two fluorine atoms on each ending group, 5,6-isomer of IDTT2OT-2F showed slightly larger dipole moment than 5,5 and 6,6 isomers. However, owing to the maintenance of the planar backbone, the three NFAs exhibit near-zero dipole moments (Table S1).

3.2. Thermal properties

The thermal properties of the three NFAs were investigated by thermogravimetric analysis (TGA) and differential scanning calorimetry (DSC) (Fig. S13). The NFAs exhibited good thermal stability with decomposition temperatures (5% weight loss) of 343, 353, and 344 $^\circ\text{C}$ for IDTT2OT, IDTT2OT-2F, and IDTT2OT-4F, respectively, which is

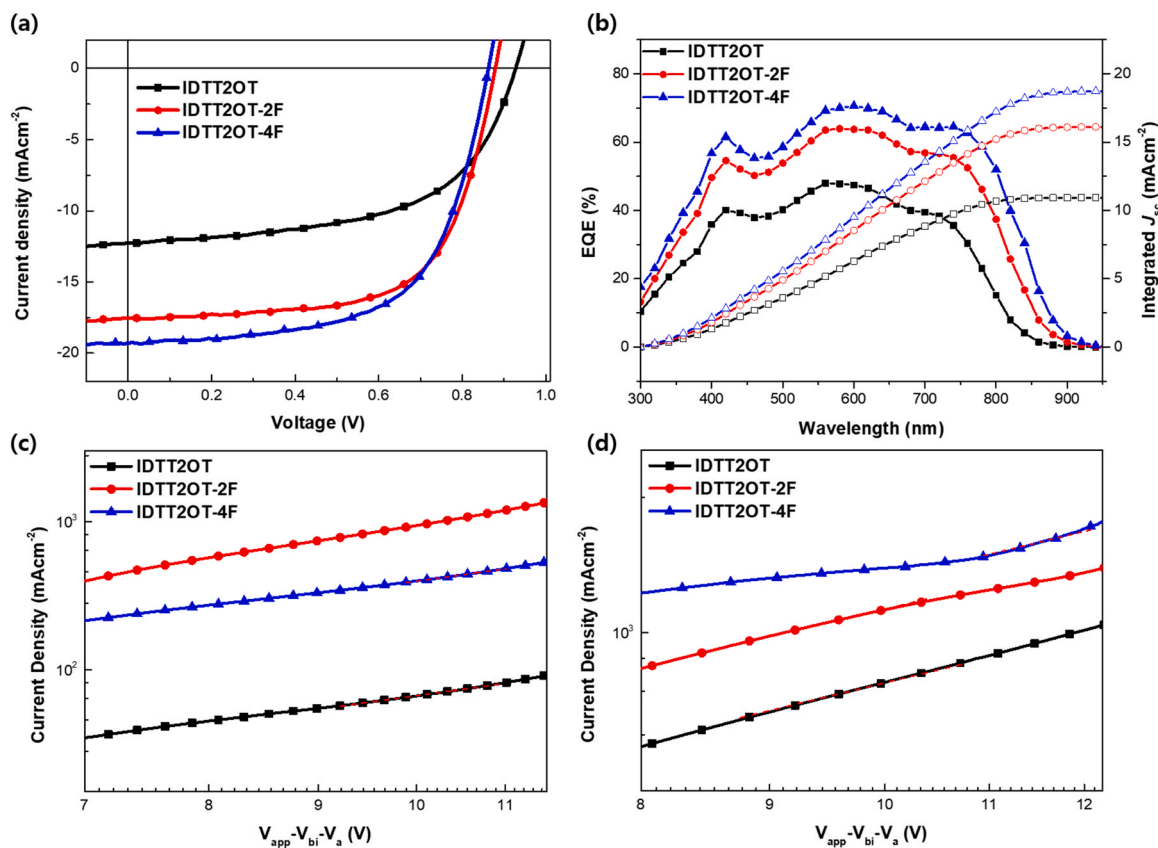


Fig. 3. (a) J-V curves, (b) EQE spectra with integrated J_{sc} , (c) electron mobility, and (d) hole mobility as obtained using SCLC methods (Red dash line is SCLC region).

Table 2
Photovoltaic parameters of IDTT2OT, IDTT2OT-2F, and IDTT2OT-4F based devices.

PBDB-T:NFA	V_{OC} (V_{OCave}^a) [V]	J_{SC} (J_{SCave}^a) [mA cm^{-2}]	J_{SC}^{cal} [mA cm^{-2}]	FF (FF_{ave}^a) [%]	PCE_{max} (PCE_{ave}^a) [%]	E_{loss} [eV]
IDTT2OT	0.93 (0.92 ± 0.01)	12.3 (12.08 ± 0.22)	10.9	56.7 (55.6 ± 1.1)	6.46 (6.36 ± 0.10)	0.58
IDTT2OT-2F	0.88 (0.87 ± 0.01)	17.5 (17.43 ± 0.12)	16.1	65.1 (64.4 ± 0.7)	10.04 (9.80 ± 0.24)	0.57
IDTT2OT-4F	0.86 (0.85 ± 0.01)	19.3 (19.12 ± 0.18)	18.7	62.4 (62.0 ± 0.4)	10.40 (10.13 ± 0.27)	0.56

^a Average values with standard deviation from over eight devices.

adequate for photovoltaic devices. The DSC curves of IDTT2OT and IDTT2OT-2F showed exothermic peaks during the first heating scan, when partial rearrangement occurred and crystalline states were generated [47–49]. IDTT2OT displays a cold crystallization peak at ~229 °C, whereas IDTT2OT-2F has peaks at ~230 °C and ~256 °C, indicating its enhanced crystallinity among the NFAs. By contrast, IDTT2OT-4F has no peak in the heating range, suggesting that it possesses the most amorphous nature among the NFAs [50].

3.3. Optical and electrochemical properties

The absorption spectra of the NFAs in chloroform and as films are shown in Fig. 2b and c and listed in Table 1. With four different dilute chloroform solutions, the molar absorption coefficient of the NFAs is calculated using the Beer–Lambert equation: $A = \epsilon bc$, where A is the absorbance, ϵ is the molar absorption coefficient, b is the length of the light path, and c is the concentration of acceptors in the solution. The average values of the molar absorption coefficient of the NFAs are measured to be 1.09×10^{-5} , 1.77×10^{-5} , and $2.03 \times 10^{-5} \text{ M}^{-1} \text{ cm}^{-1}$ at the $\lambda_{max,sol}$ values of 717, 731, and 734 nm, respectively. With their high molar absorption coefficient values at the maximized wavelength, all NFAs are expected to have effective photon harvesting ability [14]. Thin films of the NFAs exhibit broader and red-shifted absorption than those in solution; the absorption edges of the NFAs are located at 820, 856, and 873 nm, corresponding to the narrow optical bandgaps of 1.51, 1.45, and 1.42 eV, respectively.

The electrochemical properties of NFAs were investigated by cyclic voltammetry (CV) (Fig. S14). From the measured onset oxidation potential E_{onset}^{ox} values, the HOMO energies of IDTT2OT, IDTT2OT-2F, and IDTT2OT-4F were calculated to be -5.20, -5.28, and -5.32 eV and the LUMO energies to be -3.69, -3.83, and -3.90 eV, respectively (Table 1). As co-facial stacking between the molecules increases with the number of fluorine atoms, the frontier energy levels of the NFAs are lowered and the bandgaps narrowed [6].

Poly[2,6-4,8-bis(5-(2-ethylhexyl)thiophen-2-yl)-benzo-1,2-b:4,5-b1']dithiophene]-alt-(5,5-(1,3'-di-2-thienyl-5',7'-bis(2-ethylhexyl)benzo[1',2'-c:4',5'-c']dithiophene-4,8-dione)) (PBDB-T) was selected as donor owing to its strong absorption in the 500–700 nm range, which complements the NFAs' absorption (Fig. S15). The HOMO and LUMO energy levels of PBDB-T were calculated to be -5.27 eV and -3.48 eV, respectively. IDTT2OT-2F and IDTT2OT-4F display well-matched energy level alignments, whereas a small negative HOMO offset exists for IDTT2OT, which may not be beneficial for hole transfer between donor and acceptor [30].

3.4. Photovoltaic properties

Inverted-structured OSCs were fabricated with ITO/ZnO/PBDB-T:NFA/MoO₃/Ag architecture. The devices were optimized by thermal annealing at 100 °C for 10 min and high-boiling point solvent additives such as 1,8-diiodooctane (DIO), 1-chloronaphthalene (CN), and diphenyl ether (DPE) were used for enhancing the bulk-heterojunction morphology through the formation of a bicontinuous interpenetrating network [51]. The J - V curves of the best performing NFA-based devices are displayed in Fig. 3a and their photovoltaic parameters are listed in

Table 2. The IDTT2OT-4F devices exhibited J_{SC} of 19.3 mA cm^{-2} , V_{OC} of 0.86 V, FF of 62.4%, and PCE of 10.40%; these values represented the best performance among the NFA devices. In the case of the IDTT2OT device, a moderate PCE was obtained, although the device exhibited a negative HOMO offset with the donor and thereby insufficient driving force for charge transfer. With more fluorine substitution, the reduced energy bandgaps of IDTT2OT-2F and IDTT2OT-4F resulted in enhanced photo-responses, whereas the smaller gap between donor HOMO and acceptor LUMO caused V_{OC} to drop. Nevertheless, the IDTT2OT-4F device showed the most extended photon absorption, with a PCE of 10.40%, among the NFAs. With the high-lying LUMO energy level strategy, the small E_{loss} of 0.56 eV for the IDTT2OT-4F device compensates its decrease in V_{OC} , thereby providing an overall PCE boost for the OSCs via enhanced photon absorption [5,41].

External quantum efficiency (EQE) measurements were conducted for the optimized devices built using each of the acceptors and PBDB-T, and the corresponding curves are presented in Fig. 3b and Table 2. For the three devices, the entire EQE response occurs between 300 nm and 900 nm, signifying that the PBDB-T polymer donor and all three NFAs simultaneously contribute to the J_{SC} values, in agreement with the J - V characteristics. Specifically, as the IDTT2OT-4F has the most extended absorption in the NIR region, the highest EQE response was obtained for the PBDB-T:IDTT2OT-4F device.

3.5. Charge transfer and mobilities

Charge transfer and photo-induced exciton dissociation was monitored using photoluminescence (PL) spectroscopy. Spectra of the pristine PBDB-T, IDTT2OT, IDTT2OT-2F, and IDTT2OT-4F and optimized blended films were measured, with excitation at 550 nm for donor and 650 nm for acceptor, respectively, as shown in Fig. S16. (Notice: The PL measurement was performed at each wavelength which might to be showed relatively weaker PL quenching rates, owing to the tool is restricted up to 900 nm; However, its measured trends showed quite precise.) The PL quenching efficiencies of the PBDB-T:IDTT2OT, PBDB-T:IDTT2OT-2F, and PBDB-T:IDTT2OT-4F films were measured to be 65%, 67%, and 68%, respectively, at 550 nm and 68%, 73%, and 80%, respectively, at 650 nm. As the increased quenching in the blends promotes photo-induced charge transfer, the IDTT2OT-4F blend film exhibits most effective electron transfer from donor to acceptor, which is consistent with its best photovoltaic performance [52]. Interestingly, the IDTT2OT blend film exhibited a quenching rate comparable with the other blend films at both excitation wavelengths, although the blend has a negative HOMO offset, which could result in slower hole transfer and lower efficiency [35,53].

The space-charge-limited current (SCLC) method was adopted (Fig. 3c and d) and the charge mobilities were determined by fitting the dark current according to the modified Mott-Gurney equation [14,27]. In the $J = 9\epsilon_r\epsilon_0\mu_{eff}V^2/8L^3$, J is the dark current density (mA cm^{-2}), ϵ_r is the permittivity of free space ($8.85 \times 10^{-12} \text{ F cm}^{-1}$), ϵ_0 is the dielectric constant of the blend material (assumed to be 3.0), μ_{eff} is the carrier mobility, V is the effective voltage, and L is the thickness of the active layer (120 nm).

The electron-only devices with ITO/ZnO/PBDB-T:NFA/PDINO/Ag structures and hole-only devices with ITO/PEDOT:PSS/PBDB-T:NFA/

Table 3

Electron and hole mobilities of the IDTT2OT, IDTT2OT-2F, and IDTT2OT-4F based films.

PBDB-T:NFAAs	μ_e [$\text{cm}^2 \text{V}^{-1} \text{s}^{-1}$]	μ_h [$\text{cm}^2 \text{V}^{-1} \text{s}^{-1}$]	μ_e/μ_h
IDTT2OT	1.08×10^{-4}	3.02×10^{-4}	0.358
IDTT2OT-2F	8.17×10^{-4}	6.62×10^{-4}	1.234
IDTT2OT-4F	6.45×10^{-4}	8.52×10^{-4}	0.757

PEDOT:PSS/Ag structures were fabricated, and each of the observed mobilities is listed in Table 3. The PBDB-T:IDTT2OT-2F device possessed the most balanced μ_e/μ_h value of 1.23 with electron mobility of $8.17 \times 10^{-4} \text{ cm}^2 \text{V}^{-1} \text{s}^{-1}$ and hole mobility of $6.62 \times 10^{-4} \text{ cm}^2 \text{V}^{-1} \text{s}^{-1}$, which indicates enhanced structural order for the blend and better charge extraction [18]. Moreover, with its negative HOMO offset, the PBDB-T:IDTT2OT device has imbalanced mobilities, which hampers further J_{SC} improvement [54]. The PL quenching and SCLC results demonstrate the validity of introducing 3,4-dimethoxythiophene, an

effective strategy for charge separation in the device, although the energy level impedes effective charge transfer.

For providing insight of carrier recombination characteristics, light intensity dependence of J_{SC} and V_{OC} , dark current density–voltage properties were analyzed as shown in Figs. S17–S18 [55–58]. For illumination intensity (I), the equations of $J_{\text{SC}} \propto I^\alpha$ and $V_{\text{OC}} \propto kT/q \ln(I)$ exhibits suppressed carrier recombination with slope values approaching 1.0 (where, k is Boltzmann constant, T is the absolute temperature, and q is the elementary charge). In the J_{SC} -light intensity graph (Fig. S17a), slope(α) is close to 1 in the order of IDTT2OT-4F, IDTT2OT-2F, and IDTT2OT ($\alpha = 0.846, 0.835, 0.825$). In general, as α is closer to 1, bimolecular recombination tends to decrease, which is consistent with the J_{SC} trend in the photovoltaic table (18.7 mA cm^{-2} , 16.1 mA cm^{-2} , 10.9 mA cm^{-2}). In the V_{OC} -light intensity graph (Fig. S17b), the slope kT/q is close to 1 in the order of IDTT2OT, IDTT2OT-2F, and IDTT2OT-4F (slope = $1.051 kT/q, 1.056 kT/q, 1.059 kT/q$). In general, as kT/q is closer to 1, trap-assisted recombination tends to decrease, which is consistent with the V_{OC} trend in the photovoltaic table (0.93 V, 0.88 V, 0.86 V). Also, in dark current

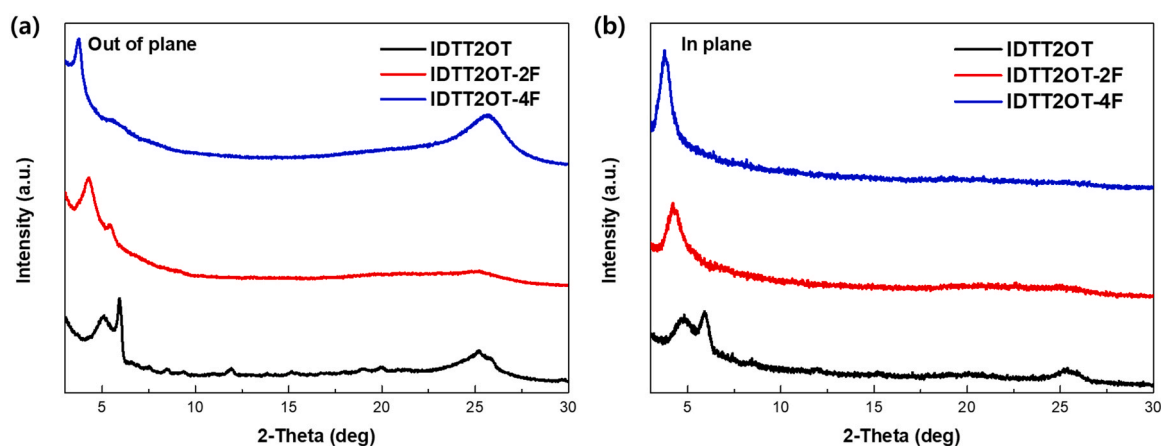


Fig. 4. XRD images of IDTT2OT, IDTT2OT-2F, and IDTT2OT-4F acquired with (a) out-of-plane and (b) in-plane irradiation.

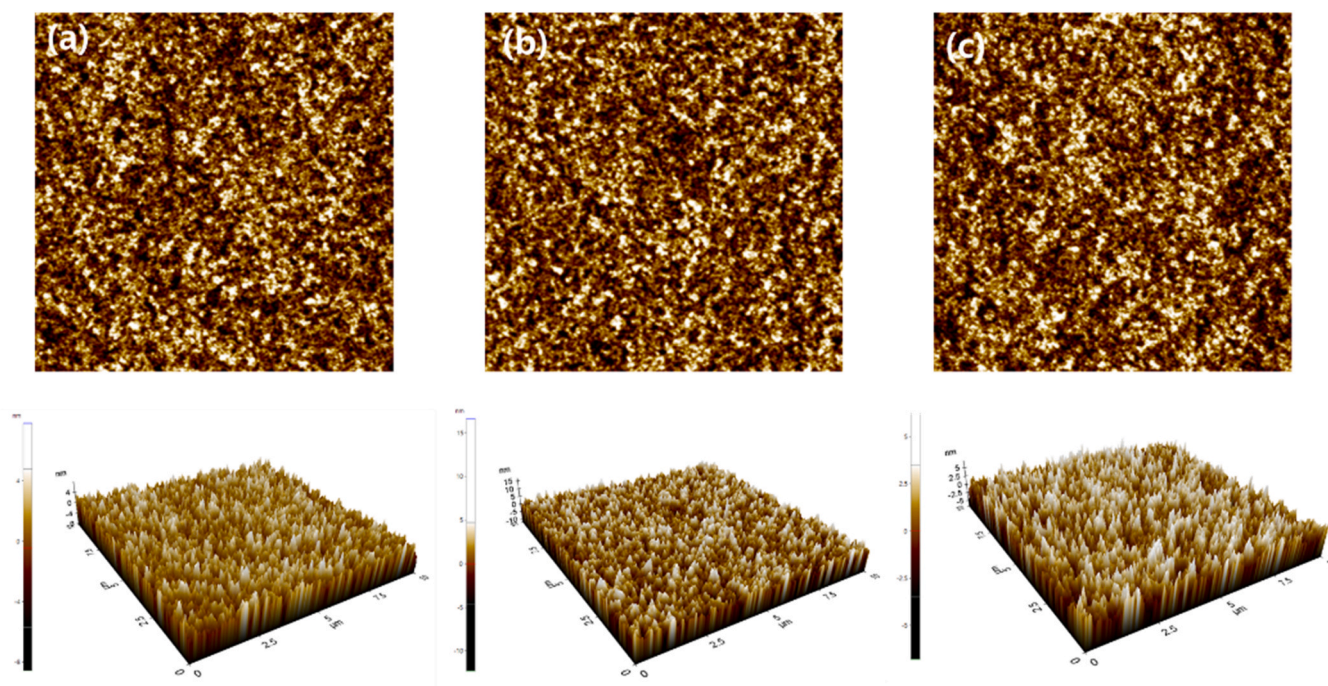


Fig. 5. The AFM height and 3D topographic images ($10 \mu\text{m} \times 10 \mu\text{m}$) of (a) PBDB-T:IDTT2OT, (b) PBDB-T:IDTT2OT-2F, and (c) PBDB-T:IDTT2OT-4F.

density-voltage graph (Fig. S18), the current density is larger from forward bias to IDTT2OT-4F, IDTT2OT-2F, and IDTT2OT, and the result is consistent with the J_{SC} values. For Reverse bias, the leakage current is small in order IDTT2OT-4F, IDTT2OT-2F, and IDTT2OT. These results showed the decrease in recombination, current density due to leakage current is less likely to occur in IDTT2OT-4F.

3.6. Structural order and morphology

As nanostructured ordering effects, from exciton diffusion to charge collection, are correlated with the performance of the device [48], solid state of the pristine NFAs film were studied by X-ray diffraction (XRD). This method allowed identification of the crystalline texture through the diffraction peak structure (Fig. 4). From the out-of-plane (OOP) irradiation measurement, (100) lamellar d-spacings (d_1) of 17.36, 20.67, and 23.60 Å were obtained for the pure-NFA films. The (010) π - π stacking diffraction peak, with distances of 3.51, 3.54, and 3.46 Å, respectively, indicates face-to-face stacking behavior [45]. The shortest π - π stacking distance of IDTT2OT-4F indicates that the introduction of fluorine atoms to the molecular backbone enables the formation of compact packing via stronger interchain networks [13,59]. Moreover, the intense (010) peak in the spectrum of the IDTT2OT-4F film, which becomes faint in the in-plane (IP) direction, demonstrates the predominant face-on orientation [17,44]. With the preferential face-on orientation and the short π - π stacking distance, the IDTT2OT-4F film exhibits superior charge transport and exciton extraction, which contribute to the elevated J_{SC} when it is incorporated into photovoltaic devices [41]. Intense (100), (001) backbone, and (010) diffraction peaks are observed in both the OOP and IP directions for the pristine IDTT2OT film, suggesting bimodal edge-on and face-on crystallites [14,44]. The observable (100) and (001) peaks in the OOP and IP spectra and faint (010) peak in the OOP spectrum, which does not appear in the IP spectrum, suggest that IDTT2OT-2F exhibits crystallinity, but with quiet disordered orientation and a relatively large stacking distance for the existence of isomers.

The morphologies of the PBDB-T:NFA thin films were measured by using atomic force microscopy (AFM) (Fig. 5) [18,45]. All the blended films for the PBDB-T:IDTT2OT, PBDB-T:IDTT2OT-2F, and PBDB-T:IDTT2OT-4F exhibited smooth surface features with comparable root-mean-square (RMS) roughness values of 1.75, 2.12, and 1.69 nm, respectively, which implies well-mixed interpenetrating networks of donor and acceptor. This trend is also reflected in the phase images as shown in Fig. S19. Larger RMS roughness values relatively correspond to reduced charge-carrier transport [20,60]. Among the blends, the IDTT2OT-4F blended film exhibited the lowest RMS roughness. Moreover, its rod-like sharp surface forms an efficient interfacial contact with electrode, which is beneficial for exciton generation and charge transfer, and thus results in the enhancement of the J_{SC} [61,62].

4. Conclusion

In summary, 3,4-dimethoxythiophene-based NFAs of IDTT2OT, IDTT2OT-2F, and IDTT2OT-4F were newly designed and synthesized to narrow the energy bandgap and increase the LUMO energy level. Through moderate fluorination within the end groups of the acceptors, enhanced absorption spectra in the NIR region were observed for the NFAs, thereby enhancing the photo-response of solar cell devices. With the best results in terms of the photocurrent and V_{OC} , the IDTT2OT-4F based device exhibits the photovoltaic performance of 10.40% with J_{SC} of 19.3 mA cm⁻², V_{OC} of 0.86 V, and FF of 62.4%, which indicates the highest PCE among the three NFAs. With its preferential face-on orientation, IDTT2OT-4F exhibits good mixing with the crystalline PBDB-T donor polymer, yielding the highest and most balanced charge transfer and mobility. Our results demonstrate that selecting the 3,4-dimethoxythiophene moiety and enhancing the electron-donating properties of the acceptors, by enlarging the NIR absorption band and

increasing the LUMO energy level, is an efficient energy level modulation strategy in NFAs for improving the photovoltaic performance of NFA-based OSCs.

CRediT authorship contribution statement

Ie Na Kim: Involved in synthesis of materials and preparation of manuscript based on the obtained results. **Sung Jae Jeon:** Involved in synthesis of materials, preparation of manuscript based on the obtained results and Writing – review & editing. **Young Hoon Kim:** Preparation of manuscript based on the obtained results, helped to interpret the data and Writing – review & editing. **Hyung Seok Lee:** Fabricated the devices and helped to interpret the data. **Yong Woon Han:** Writing – review & editing. **Nam Gyu Yang:** Preparation of manuscript based on the obtained results and Writing – review & editing. **Dong Hyeon Hong:** Preparation of manuscript based on the obtained results and Writing – review & editing. **Chang Ho Jung:** Preparation of manuscript based on the obtained results and Writing – review & editing. **Doo Kyung Moon:** Made overall correction, management and coordination responsibility for the research activity planning and experiment.

Declaration of Competing Interest

The authors declare that they have no known competing financial interests or personal relationships that could have appeared to influence the work reported in this paper.

Acknowledgments

This paper was supported by Konkuk University in 2019. This research was supported by the Korea Institute of Energy Technology Evaluation and Planning (KETEP) and the Ministry of Trade, Industry & Energy (MOTIE) of the Republic of Korea (No. 20193091010110), the National Research Foundation of Korea (NRF) grant funded by the Korea government (MSIT) (No. 2020R1A2C201091611), and the Human Resources Program (No. 20194010201790) of the Korea Institute of Energy Technology Evaluation and Planning (KETEP).

Appendix A. Supporting information

Supplementary data associated with this article can be found in the online version at doi:10.1016/j.synthmet.2021.116880.

References

- [1] G. Yu, J. Gao, J.C. Hummelen, F. Wudl, A.J. Heeger, Polymer photovoltaic cells: enhanced efficiencies via a network of internal donor-acceptor heterojunctions, *Science* 270 (1995) 1789–1791, <https://doi.org/10.1126/science.270.5243.1789>.
- [2] N. Bauer, Q. Zhang, J. Zhao, L. Ye, J.H. Kim, I. Constantinou, L. Yan, F. So, H. Ade, H. Yan, W. You, Comparing non-fullerene acceptors with fullerene in polymer solar cells: a case study with FTAZ and PycNTAZ, *J. Mater. Chem. A* 5 (2017) 4886–4893, <https://doi.org/10.1039/c6ta10450a>.
- [3] B. Zheng, L. Huo, Y. Li, Benzodithiophenedione-based polymers: recent advances in organic photovoltaics, *NPG Asia Mater.* 12 (2020) 3, <https://doi.org/10.1038/s41427-019-0163-5>.
- [4] J. Yuan, Y. Zhang, L. Zhou, G. Zhang, H.L. Yip, T.K. Lau, X. Lu, C. Zhu, H. Peng, P. A. Johnson, M. Leclerc, Y. Cao, J. Ulanski, Y. Li, Y. Zou, Single-junction organic solar cell with over 15% efficiency using fused-ring acceptor with electron-deficient core, *Joule* 3 (2019) 1140–1151, <https://doi.org/10.1016/j.joule.2019.01.004>.
- [5] Y. Ma, M. Zhang, Y. Tang, W. Ma, Q. Zheng, Angular-shaped dithienonaphthalene-based nonfullerene acceptor for high-performance polymer solar cells with large open-circuit voltages and minimal energy losses, *Chem. Mater.* 29 (2017) 9775–9785, <https://doi.org/10.1021/acs.chemmater.7b03770>.
- [6] Z. Wang, K. Huang, X. Chen, Y. Xu, Z. Xu, T. He, S. Yin, H. Qiu, M. Li, Q. Zhang, A high-performance non-fullerene electron acceptor with bisalkylthiophene π -bridges for organic photovoltaics, *J. Mater. Chem. C* 7 (2019) 14499–14503, <https://doi.org/10.1039/c9tc05166j>.
- [7] P. Cheng, G. Li, X. Zhan, Y. Yang, Next-generation organic photovoltaics based on non-fullerene acceptors /639/301/299/946 /639/624/399 review-article, *Nat. Photonics* 12 (2018) 131–142, <https://doi.org/10.1038/s41566-018-0104-9>.

- [8] Y. Lin, Z.G. Zhang, H. Bai, J. Wang, Y. Yao, Y. Li, D. Zhu, X. Zhan, High-performance fullerene-free polymer solar cells with 6.31% efficiency, *Energy Environ. Sci.* 8 (2015) 610–616, <https://doi.org/10.1039/c4ee03424d>.
- [9] T.H. Lee, D.H. Kim, E.J. Lee, D.K. Moon, Significant impact of monomer curvatures for polymer curved shape composition on backbone orientation and solar cell performances, *J. Ind. Eng. Chem.* 65 (2018) 195–204, <https://doi.org/10.1016/j.jiec.2018.04.029>.
- [10] Y. Liu, C. Zhang, D. Hao, Z. Zhang, L. Wu, M. Li, S. Feng, X. Xu, F. Liu, X. Chen, Z. Bo, Enhancing the performance of organic solar cells by hierarchically supramolecular self-assembly of fused-ring electron acceptors, *Chem. Mater.* 30 (2018) 4307–4312, <https://doi.org/10.1021/acs.chemmater.8b01319>.
- [11] P. Yin, L. Wang, J. Liang, Y. Yu, L. Chen, C. Weng, C. Cui, P. Shen, A small-molecule/fullerene acceptor alloy: a powerful tool to enhance the device efficiency and thermal stability of ternary polymer solar cells, *J. Mater. Chem. C* 8 (2020) 11223–11238, <https://doi.org/10.1039/d0tc00329h>.
- [12] D. Liu, T. Wang, X. Ke, N. Zheng, Z. Chang, Z. Xie, Y. Liu, Ultra-narrow bandgap non-fullerene acceptors for organic solar cells with low energy loss, *Mater. Chem. Front.* 3 (2019) 2157–2163, <https://doi.org/10.1039/c9qm00505f>.
- [13] D. Su, K. Li, W. Liu, W. Zhang, X. Li, Y. Wu, F. Shen, S. Huo, H. Fu, C. Zhan, High-performance ternary polymer solar cells enabled by a new narrow bandgap nonfullerene small molecule acceptor with a higher LUMO level, *Macromol. Rapid Commun.* 41 (2020) 1–10, <https://doi.org/10.1002/marc.202000393>.
- [14] J.E. Yu, S.J. Jeon, J.Y. Choi, Y.W. Han, E.J. Ko, D.K. Moon, A 3-fluoro-4-hexylthiophene-based wide bandgap donor polymer for 10.9% efficiency eco-friendly nonfullerene organic solar cells, *Small* 15 (2019) 1–10, <https://doi.org/10.1002/smll.201805321>.
- [15] Z. Luo, R. Ma, Z. Chen, Y. Xiao, G. Zhang, T. Liu, R. Sun, Q. Zhan, Y. Zou, C. Zhong, Y. Chen, H. Sun, G. Chai, K. Chen, X. Guo, J. Min, X. Lu, C. Yang, H. Yan, Altering the positions of chlorine and bromine substitution on the end group enables high-performance acceptor and efficient organic solar cells, *Adv. Energy Mater.* 10 (2020) 1–8, <https://doi.org/10.1002/aenm.202002649>.
- [16] T. Liu, Y. Zhang, Y. Shao, R. Ma, Z. Luo, Y. Xiao, T. Yang, X. Lu, Z. Yuan, H. Yan, Y. Chen, Y. Li, Asymmetric acceptors with fluorine and chlorine substitution for organic solar cells toward 16.83% efficiency, *Adv. Funct. Mater.* 30 (2020), <https://doi.org/10.1002/adfm.202000456>.
- [17] Z. Zhang, W. Liu, T. Rehman, H.-X. Ju, J. Mai, X. Lu, M. Shi, J. Zhu, C.Z. Li, H. Chen, Energy-level modulation of non-fullerene acceptors to achieve high-efficiency polymer solar cells at a diminished energy offset, *J. Mater. Chem. A* 5 (2017) 9649–9654, <https://doi.org/10.1039/c7ta01554b>.
- [18] J. Lee, S.J. Ko, M. Seifrid, H. Lee, B.R. Luginbuhl, A. Karki, M. Ford, K. Rosenthal, K. Cho, T.Q. Nguyen, G.C. Bazan, Bandgap narrowing in non-fullerene acceptors: single atom substitution leads to high optoelectronic response beyond 1000 nm, *Adv. Energy Mater.* 8 (2018) 1–6, <https://doi.org/10.1002/aenm.201801212>.
- [19] X. Shi, J. Chen, K. Gao, L. Zuo, Z. Yao, F. Liu, J. Tang, A.K.Y. Jen, Terthieno[3,2-*b*] Thiophene (6T) based low bandgap fused-ring electron acceptor for highly efficient solar cells with a high short-circuit current density and low open-circuit voltage loss, *Adv. Energy Mater.* 8 (2018) 2–9, <https://doi.org/10.1002/aenm.201702831>.
- [20] Y. Cui, H. Yao, J. Zhang, K. Xian, T. Zhang, L. Hong, Y. Wang, Y. Xu, K. Ma, C. An, C. He, Z. Wei, F. Gao, J. Hou, Single-junction organic photovoltaic cells with approaching 18% efficiency, *Adv. Mater.* 32 (2020) 1–7, <https://doi.org/10.1002/adma.201908205>.
- [21] S.J. Ko, Q.V. Hoang, C.E. Song, M.A. Uddin, E. Lim, S.Y. Park, B.H. Lee, S. Song, S. J. Moon, S. Hwang, P.O. Morin, M. Leclerc, G.M. Su, M.L. Chabinyk, H.Y. Woo, W. S. Shin, J.Y. Kim, High-efficiency photovoltaic cells with wide optical band gap polymers based on fluorinated phenylene-alkoxybenzothiadiazole, *Energy Environ. Sci.* 10 (2017) 1443–1455, <https://doi.org/10.1039/c6ee03051c>.
- [22] B. Xiao, A. Tang, J. Zhang, A. Mahmood, Z. Wei, E. Zhou, Achievement of high Voc of 1.02 V for P3HT-based organic solar cell using a benzotriazole-containing non-fullerene acceptor, *Adv. Energy Mater.* 7 (2017) 1–7, <https://doi.org/10.1002/aenm.201602269>.
- [23] A. Tang, W. Song, B. Xiao, J. Guo, J. Min, Z. Ge, J. Zhang, Z. Wei, E. Zhou, Benzotriazole-based acceptor and donors, coupled with chlorination, achieve a high Voc of 1.24 V and an efficiency of 10.5% in fullerene-free organic solar cells, *Chem. Mater.* 31 (2019) 3941–3947, <https://doi.org/10.1021/acs.chemmater.8b05316>.
- [24] B. Xiao, A. Tang, J. Yang, A. Mahmood, X. Sun, E. Zhou, Quinoxaline-containing nonfullerene small-molecule acceptors with a linear A2-A1-D-A1-A2 skeleton for Poly(3-hexylthiophene)-based organic solar cells, *ACS Appl. Mater. Interfaces* 10 (2018) 10254–10261, <https://doi.org/10.1021/acsami.8b00216>.
- [25] B. Xiao, Q. Zhang, G. Li, M. Du, Y. Geng, X. Sun, A. Tang, Y. Liu, Q. Guo, E. Zhou, Side chain engineering of quinoxaline-based small molecular nonfullerene acceptors for high-performance poly(3-hexylthiophene)-based organic solar cells, *Sci. China Chem.* 63 (2020) 254–264, <https://doi.org/10.1007/s11426-019-9618-7>.
- [26] J. Li, C. Sun, A. Tang, B. Zhang, Q. Guo, E. Zhou, Y. Li, Utilizing an electron-deficient thieno[3,4-*c*] pyrrole-4,6-dione (TPD) unit as a π -bridge to improve the photovoltaic performance of A- π -D- π -A type acceptors, *J. Mater. Chem. C* 8 (2020) 15981–15984, <https://doi.org/10.1039/d0tc04601a>.
- [27] Y.W. Han, H.J. Song, S.J. Jeon, H.S. Lee, E.J. Ko, C.E. Song, T.H. Sung, D.K. Moon, Excellent carrier transport materials produced by controlled molecular stacking and their application in flexible organic electronic devices, *J. Mater. Chem. A* 7 (2019) 14790–14805, <https://doi.org/10.1039/c9ta02213a>.
- [28] Y. Chang, X. Zhang, Y. Tang, M. Gupta, D. Su, J. Liang, D. Yan, K. Li, X. Guo, W. Ma, H. Yan, C. Zhan, 14%-Efficiency fullerene-free ternary solar cell enabled by designing a short side-chain substituted small-molecule acceptor, *Nano Energy* 64 (2019), 103934, <https://doi.org/10.1016/j.nanoen.2019.103934>.
- [29] P. Jiang, S. Ming, Q.Q. Jia, Y. Liu, H. Lu, M. Li, X. Xu, H.B. Li, Z. Bo, The influence of the π -bridging unit of fused-ring acceptors on the performance of organic solar cells, *J. Mater. Chem. A* 6 (2018) 21335–21340, <https://doi.org/10.1039/c8ta08410f>.
- [30] K. Cnops, G. Zango, J. Genoe, P. Heremans, M.V. Martinez-Diaz, T. Torres, D. Cheyns, Energy level tuning of non-fullerene acceptors in organic solar cells, *J. Am. Chem. Soc.* 137 (2015) 8991–8997, <https://doi.org/10.1021/jacs.5b02808>.
- [31] M. Ghasemi, H. Hu, Z. Peng, J.J. Rech, I. Angunawela, J.H. Carpenter, S.J. Stuard, A. Wadsworth, I. McCulloch, W. You, H. Ade, Delineation of thermodynamic and kinetic factors that control stability in non-fullerene organic solar cells, *Joule* 3 (2019) 1328–1348, <https://doi.org/10.1016/j.joule.2019.03.020>.
- [32] K.R. Graham, P. Erwin, D. Nordlund, K. Vandewal, R. Li, G.O. Ngongang Ndjawa, E.T. Hoke, A. Salleo, M.E. Thompson, M.D. McGehee, A. Amassian, Re-evaluating the role of sterics and electronic coupling in determining the open-circuit voltage of organic solar cells, *Adv. Mater.* 25 (2013) 6076–6082, <https://doi.org/10.1002/adma.201301319>.
- [33] S. Li, L. Ye, W. Zhao, S. Zhang, S. Mukherjee, H. Ade, J. Hou, Energy-level modulation of small-molecule electron acceptors to achieve over 12% efficiency in polymer solar cells, *Adv. Mater.* 28 (2016) 9423–9429, <https://doi.org/10.1002/adma.201602776>.
- [34] G.P. Kini, J.Y. Choi, S.J. Jeon, I.S. Suh, D.K. Moon, Controlling the interchain packing and photovoltaic properties via fluorine substitution in terpolymers based on benzo[1,2-*c*:4,5-*c'*]dithiophene-4,8-dione and benzothiadiazole units, *Polymer* 148 (2018) 330–338, <https://doi.org/10.1016/j.polymer.2018.06.038>.
- [35] Z. Zhang, H. Wang, J. Yu, R. Sun, J. Xu, L. Yang, R. Geng, J. Cao, F. Du, J. Min, F. Liu, W. Tang, Modification on the Indacenodithieno[3,2-*b*]thiophene core to achieve higher current and reduced energy loss for nonfullerene solar cells, *Chem. Mater.* 32 (2020) 1297–1307, <https://doi.org/10.1021/acs.chemmater.9b04911>.
- [36] T. Liu, R. Ma, Z. Luo, Y. Guo, G. Zhang, Y. Xiao, T. Yang, Y. Chen, G. Li, Y. Yi, X. Lu, H. Yan, B. Tang, Concurrent improvement in JSC and VOC in high-efficiency ternary organic solar cells enabled by a red-absorbing small-molecule acceptor with a high LUMO level, *Energy Environ. Sci.* 13 (2020) 2115–2123, <https://doi.org/10.1039/d0ee00662a>.
- [37] R. Ma, Y. Tao, Y. Chen, T. Liu, Z. Luo, Y. Guo, Y. Xiao, J. Fang, G. Zhang, X. Li, X. Guo, Y. Yi, M. Zhang, X. Lu, Y. Li, H. Yan, Achieving 16.68% efficiency ternary as-cast organic solar cells, *Sci. China Chem.* 64 (2021) 581–589, <https://doi.org/10.1007/s11426-020-9912-0>.
- [38] R. Ma, T. Yang, Y. Xiao, T. Liu, G. Zhang, Z. Luo, G. Li, X. Lu, H. Yan, B. Tang, pH gradient difference around ischemic brain tissue can serve as a trigger for delivering polyethylene glycol-conjugated urokinase nanogels, *J. Control Release* 225 (2016) 53–63, <https://doi.org/10.1002/eem2.12226>.
- [39] R. Ma, M. Zeng, Y. Li, T. Liu, Z. Luo, Y. Xu, P. Li, N. Zheng, J. Li, Y. Li, R. Chen, J. Hou, F. Huang, H. Yan, Rational anode engineering enables progresses for different types of organic solar cells, *Adv. Energy Mater.* 11 (2021) 1–11, <https://doi.org/10.1002/aenm.202100492>.
- [40] T.H. Lee, S.Y. Park, B. Walker, S.J. Ko, J. Heo, H.Y. Woo, H. Choi, J.Y. Kim, A universal processing additive for high-performance polymer solar cells, *RSC Adv.* 7 (2017) 7476–7482, <https://doi.org/10.1039/c6ra27944a>.
- [41] X. Li, T. Yan, H. Bin, G. Han, L. Xue, F. Liu, Y. Yi, Z.G. Zhang, T.P. Russell, Y. Li, Insertion of double bond π -bridges of A-D-A acceptors for high performance near-infrared polymer solar cells, *J. Mater. Chem. A* 5 (2017) 22588–22597, <https://doi.org/10.1039/c7ta07049g>.
- [42] X. Guo, F.S. Kim, S.A. Jenekhe, M.D. Watson, Phthalimide-based polymers for high performance organic thin-film transistors, *J. Am. Chem. Soc.* 131 (2009) 7206–7207, <https://doi.org/10.1021/ja810050y>.
- [43] X. Guo, J. Quinn, Z. Chen, H. Usta, Y. Zheng, Y. Xia, J.W. Hennek, R.P. Ortiz, T. J. Marks, A. Facchetti, Dialkoxymethoxy: a new building block for head-to-head polymer semiconductors, *J. Am. Chem. Soc.* 135 (2013) 1986–1996, <https://doi.org/10.1021/ja3120532>.
- [44] C. Li, Q. Yue, H. Wu, B. Li, H. Fan, X. Zhu, Small bandgap non-fullerene acceptor enables efficient PTB7-Th solar cell with near 0 eV HOMO offset, *J. Energy Chem.* 52 (2021) 60–66, <https://doi.org/10.1016/j.jechem.2020.03.058>.
- [45] Q. Liao, Y. Wang, M.A. Uddin, J. Chen, H. Guo, S. Shi, Y. Wang, H.Y. Woo, X. Guo, Drastic effects of fluorination on backbone conformation of head-to-head bithiophene-based polymer semiconductors, *ACS Macro Lett.* 7 (2018) 519–524, <https://doi.org/10.1021/acsmacrolett.8b00032>.
- [46] S.J. Nam, S.J. Jeon, Y.W. Han, D.K. Moon, Effect of non-covalent interactions on molecular stacking and photovoltaic properties in organic photovoltaics, *J. Ind. Eng. Chem.* 63 (2018) 191–200, <https://doi.org/10.1016/j.jiec.2018.02.015>.
- [47] Y. Lin, J. Wang, Z.G. Zhang, H. Bai, Y. Li, D. Zhu, X. Zhan, An electron acceptor challenging fullerenes for efficient polymer solar cells, *Adv. Mater.* 27 (2015) 1170–1174, <https://doi.org/10.1002/adma.201404317>.
- [48] H. Bin, Z.G. Zhang, L. Gao, S. Chen, L. Zhong, L. Xue, C. Yang, Y. Li, Non-fullerene polymer solar cells based on alkylthio and fluorine substituted 2D-conjugated polymers reach 9.5% efficiency, *J. Am. Chem. Soc.* 138 (2016) 4657–4664, <https://doi.org/10.1021/jacs.6b01744>.
- [49] Z. Zhang, J. Miao, Z. Ding, B. Kan, B. Lin, X. Wan, W. Ma, Y. Chen, X. Long, C. Dou, J. Zhang, J. Liu, L. Wang, Efficient and thermally stable organic solar cells based on small molecule donor and polymer acceptor, *Nat. Commun.* 10 (2019) 1–8, <https://doi.org/10.1038/s41467-019-10984-6>.
- [50] H. Zhang, S. Li, B. Xu, H. Yao, B. Yang, J. Hou, Fullerene-free polymer solar cell based on a polythiophene derivative with an unprecedented energy loss of less than 0.5 eV, *J. Mater. Chem. A* 4 (2016) 18043–18049, <https://doi.org/10.1039/c6ta06762f>.
- [51] M. Chen, D. Liu, W. Li, R.S. Gurney, D. Li, J. Cai, E.L.K. Spooner, R.C. Kilbride, J. D. McGettrick, T.M. Watson, Z. Li, R.A.L. Jones, D.G. Lidzey, T. Wang, Influences of

- non-fullerene acceptor fluorination on three-dimensional morphology and photovoltaic properties of organic solar cells, *ACS Appl. Mater. Interfaces* 11 (2019) 26194–26203, <https://doi.org/10.1021/acsami.9b07317>.
- [52] J. Xin, X. Meng, X. Xu, Q. Zhu, H.B. Naveed, W. Ma, Cold crystallization temperature correlated phase separation, performance, and stability of polymer solar cells, *Matter* 1 (2019) 1316–1330, <https://doi.org/10.1016/j.matt.2019.06.011>.
- [53] S. Li, L. Zhan, C. Sun, H. Zhu, G. Zhou, W. Yang, M. Shi, C.Z. Li, J. Hou, Y. Li, H. Chen, Highly efficient fullerene-free organic solar cells operate at near zero highest occupied molecular orbital offsets, *J. Am. Chem. Soc.* 141 (2019) 3073–3082, <https://doi.org/10.1021/jacs.8b12126>.
- [54] H. Bin, Y. Yang, Z. Peng, L. Ye, J. Yao, L. Zhong, C. Sun, L. Gao, H. Huang, X. Li, B. Qiu, L. Xue, Z.G. Zhang, H. Ade, Y. Li, Effect of alkylsilyl side-chain structure on photovoltaic properties of conjugated polymer donors, *Adv. Energy Mater.* 8 (2018) 1–8, <https://doi.org/10.1002/aenm.201702324>.
- [55] S.R. Cowan, N. Banerji, W.L. Leong, A.J. Heeger, Charge formation, recombination, and sweep-out dynamics in organic solar cells, *Adv. Funct. Mater.* 22 (2012) 1116–1128, <https://doi.org/10.1002/adfm.201101632>.
- [56] L.J.A. Koster, V.D. Mihailetschi, H. Xie, P.W.M. Blom, Origin of the light intensity dependence of the short-circuit current of polymer/fullerene solar cells, *Appl. Phys. Lett.* 87 (2005), 203502, <https://doi.org/10.1063/1.2130396>.
- [57] C.M. Proctor, T.-Q. Nguyen, Effect of leakage current and shunt resistance on the light intensity dependence of organic solar cells, *Appl. Phys. Lett.* 106 (2015), 083301, <https://doi.org/10.1063/1.4913589>.
- [58] J. Vollbrecht, V.V. Brus, S. Ko, J. Lee, A. Karki, D.X. Cao, K. Cho, G.C. Bazan, T. Nguyen, Quantifying the nongeminate recombination dynamics in nonfullerene bulk heterojunction organic solar cells, *Adv. Energy Mater.* 9 (2019), 1901438, <https://doi.org/10.1002/aenm.201901438>.
- [59] S.J. Jeon, Y.W. Han, D.K. Moon, Drastic changes in properties of donor-acceptor polymers induced by asymmetric structural isomers for application to polymer solar cells, *ACS Appl. Mater. Interfaces* 11 (2019) 9239–9250, <https://doi.org/10.1021/acsami.8b19449>.
- [60] C. McDowell, M. Abdelsamie, M.F. Toney, G.C. Bazan, Solvent additives: key morphology-directing agents for solution-processed organic solar cells, *Adv. Mater.* 30 (2018) 1–30, <https://doi.org/10.1002/adma.201707114>.
- [61] Y. Huang, E.J. Kramer, A.J. Heeger, G.C. Bazan, Bulk heterojunction solar cells: morphology and performance relationships, *Chem. Rev.* 114 (2014) 7006–7043, <https://doi.org/10.1021/cr400353v>.
- [62] Y.W. Han, S.J. Jeon, H.S. Lee, H. Park, K.S. Kim, H.W. Lee, D.K. Moon, Evaporation-free nonfullerene flexible organic solar cell modules manufactured by an all-solution process, *Adv. Energy Mater.* 9 (2019) 1–15, <https://doi.org/10.1002/aenm.201902065>.